THE BELL SYSTEM TECHNICAL JOURNAL

DEVOTED TO THE SCIENTIFIC AND ENGINEERING ASPECTS OF ELECTRICAL COMMUNICATION

Volume 62 November 1983 Number 9, Part 1

Calculation of Modes in an Optical Fiber Using the Finite Element Method and EISPACK

By T. A. LENAHAN*

(Manuscript received April 20, 1983)

This paper presents a method for computing the propagation modes of a circular optical fiber. Finite element analysis reduces Maxwell's equations to standard eigenvalue equations involving symmetric tridiagonal matrices. Routines from the Eigensystem Package (EISPACK) compute their eigenvalues and eigenvectors, and from these the waveforms, propagation constants, and delays (per unit length) of the modes are obtained. An extension allows loss of leaky modes to be calculated. Examples indicate that the method is reliable, economical, and comprehensive, applying to both single and multimode fibers.

I. INTRODUCTION

This paper presents a method for calculating the propagation modes of a circular optical fiber. The modal quantities, essential for telecommunications, include the waveforms (which describe the radial distribution of propagating power), the propagation constants (which determine cutoff conditions), and the delays per unit length (which

*Bell Laboratories.

determine pulse dispersion along the fiber). The technique combines the Finite Element Method (FEM) and routines from the Eigensystem Package (EISPACK)[1] to achieve an efficient calculation of these modal quantities for both single and multimode fibers.

The most popular approach to modal calculations for multimode fibers has been the Wentzel, Kramers, Brillouin (WKB) method, where Maxwell's equations are approximated by an easily integrated first-order differential equation.[2] WKB analysis provides a simple model for understanding optical transmission through a fiber[3] and has guided fiber design.[4]

For fibers with index of refraction profiles described by a power law, the WKB method is equivalent to geometric optics and to the model of a fiber with unlimited radial extension.[5] For such fibers the effect of the outer cladding is missed by the WKB and equivalent methods, and the bandwidth capability is often overestimated.[6]

Accuracy of the WKB method declines substantially with the number of propagating modes. For single-mode fibers the WKB method is not suitable, and instead, various analytic and numerical techniques have been used.

Analytic calculations have centered about the step-index profile and the infinitely extending parabolic profiles. Modal quantities have been expressed in terms of Bessel functions for the single step[7] and, also, the double step.[8] Parabolic profiles, analyzed by analogy with the harmonic oscillator,[9] have well-known expressions for their modal quantities. Coupled with perturbation analysis,[10] these results cover a broad range of profiles. But numerical approaches permit an even more comprehensive treatment.

Several numerical procedures have extended the analysis of the step-index profile. The solution in the core comes from a numerical integration; the solution in the cladding (where the index is assumed constant) is well known. Boundary conditions at the core-cladding interface link the two solutions and lead to a set of linear equations involving the propagation constant as a parameter. A search of the corresponding determinant for zeroes gives the propagation constants and, subsequently, the waveforms and delays.

In Ref. 11 this procedure is applied to Maxwell's first-order vector equations, and important results have been obtained for multimode[12,13] and single-mode[14,15] fibers. A similar scheme[16] deals with two coupled second-order differential equations equivalent to Maxwell's equations. The second-order scalar wave equation approximates Maxwell's equations by neglecting the relatively small gradient index terms. In Ref. 17 the basic procedure is applied to the scalar wave equation, and a variety of results have been obtained for single-mode fibers.[18,19]

In Ref. 20 the FEM is developed in terms of a variational principle

for the vector equations. Approximate solutions in the core and cladding are matched at the interface by performing a determinant search, as described before. The FEM has also been applied[21] to diverse single-mode waveguides by approximating the index profile by piecewise constant functions and then enforcing boundary conditions across the numerous interfaces. The result is a matrix eigenvalue equation in generalized form. Both of these FEM approaches seem limited to a small number of modes for economical operation.

The approach in this paper is characterized by a sequence of three steps. First, Maxwell's equations are transformed to ordinary differential equations in eigenvalue form. In one case, gradient index terms are neglected, and in the second, they are considered to first order so that their effect can be monitored. Next, finite element analysis, using the Galerkin technique,[22] reduces these differential equations to matrix equations in standard eigenvalue form. The matrices are symmetric and tridiagonal, and their positive eigenvalues correspond to the propagation modes. The routine BISECT in the EISPACK[1] library delivers the eigenvalues and TINVIT, also in EISPACK, delivers the corresponding eigenvectors. The eigenvalues give the propagation constants of the modes, the eigenvectors give the waveforms, and a combination of the two give the delays.

Like many other numerical techniques, this method can treat any uniform, circular fiber and meet usual standards of accuracy. Also, the effect of gradient index terms can be monitored. But by casting the equations in standard eigenvalue form, modern techniques of computational linear algebra (as used in EISPACK) can achieve substantial cost advantage over other numerical approaches. Typically, this method will process for a multimode fiber 25 modes per second on the *Cray-1** computer.

The calculation procedure is derived in the next section. Effects of material dispersion are incorporated into the analysis, and calculation of loss for leaky modes is also considered. Results are given in Section III for a variety of single and multimode examples. These results, as discussed in Section IV, illustrate the reliability, economy, and scope of the method.

II. ANALYSIS

This section derives from Maxwell's equations an algorithm that computes the propagation modes of an optical fiber. The algorithm is straightforward and can be carried out on any computer that has access to the EISPACK[1] or similar routines.

---

* Registered service mark of Cray Research, Inc.

2.1 Reduction of Maxwell's equations

The fiber is assumed perfectly straight and circular, and uniform along its length. The cylindrical coordinate system (r, θ, z) is defined so that the z-axis coincides with the fiber axis. The index of refraction can then be expressed by the function $n(r)$, the index profile. The profile can be any bounded function in the core ($r \leq R_1$), but it is constant (n_{cl}) in the cladding. The geometry is shown in Fig. 1.

The permittivity is

$$\epsilon = \epsilon_o n^2(r), \tag{1}$$

where ϵ_o denotes the free-space permittivity. The permeability μ is assumed throughout to be μ_o, the free-space value.

Maxwell's equations relate the electric field E and the magnetic field H by

$$\begin{aligned} \text{curl } E &= -i\omega\mu H \\ \text{curl } H &= i\omega\epsilon E, \end{aligned} \tag{2}$$

where ω denotes the frequency of excitation (in rad/s). Taking the curl of the second equation eliminates E to give

$$\nabla^2 H + \nabla g \times (\nabla \times H) + k^2 H = 0, \tag{3}$$

where

$$g = \ln(k^2), \tag{4}$$

and the wave number k has the forms

$$k = \omega(\mu\epsilon)^{1/2} = \omega n(\mu_o\epsilon_o)^{1/2} = \omega n/c = 2\pi n/\lambda, \tag{5}$$

with n the index of refraction, c the velocity of light in vacuum, and λ the free-space wavelength of the excitation.

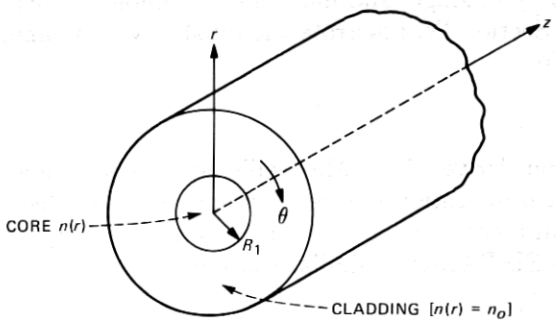

Fig. 1—Geometry of a uniform circular fiber with index profile $n(r)$.

Propagation modes are solutions of the form

$$H = H_o \exp(i\beta z), \tag{6}$$

where H_o is a vector field independent of z, and β is the propagation constant of the mode. Substituting this into the field equation gives, in cylindrical coordinates,

$$\begin{bmatrix} \Delta^2 - \frac{1}{r^2} + k^2 - \frac{g_r}{r}\frac{\partial}{\partial r} & r\left(\frac{2}{r^2} + \frac{g_r}{r}\right)\frac{\partial}{\partial \theta} & 0 \\ -\frac{2}{r^2}\frac{\partial}{\partial \theta} & \nabla^2 - \frac{1}{r^2} + k^2 & 0 \\ 0 & i\beta g_r & \nabla^2 - g_r\frac{\partial}{\partial r} + k^2 \end{bmatrix} \begin{pmatrix} H_{o\theta} \\ H_{or} \\ H_{oz} \end{pmatrix} = \beta^2 \begin{pmatrix} H_{o\theta} \\ H_{or} \\ H_{oz} \end{pmatrix}, \tag{7}$$

where g_r means $\partial g/\partial r$. The transverse (i.e., r and θ) components of H are uncoupled from the longitudinal (i.e., z) component and satisfy an eigenvalue equation with eigenvalue β^2. The corresponding operators are indicated as a 2×2 submatrix in the full 3×3 matrix.

The angular dependence of the transverse field is given by

$$\begin{pmatrix} H_{o\theta} \\ H_{or} \end{pmatrix} = \begin{pmatrix} h_\theta \cos m'\theta \\ h_r \sin m'\theta \end{pmatrix} \quad \text{or} \quad \begin{pmatrix} h_\theta \sin m'\theta \\ h_r \cos m'\theta \end{pmatrix}$$

$$\text{for} \quad m' = 0, 1, 2, \cdots, \tag{8}$$

where the functions h_θ and h_r depend only on r. The two forms correspond to different polarizations. Substituting these into eq. (7) gives

$$\begin{bmatrix} \left(\frac{1}{r}\frac{d}{dr} r \frac{d}{dr} - \frac{g_r}{r}\frac{d}{dr} - \frac{m'^2 + 1}{r^2} + k^2\right) \pm m'\left(\frac{2}{r^2} + \frac{g_r}{r}\right) \\ \pm \frac{2m'}{r^2} \qquad \left(\frac{1}{r}\frac{d}{dr} r \frac{d}{dr} - \frac{m'^2 + 1}{r^2} + k^2\right) \end{bmatrix} \cdot \begin{pmatrix} h_\theta \\ h_r \end{pmatrix} = \beta^2 \begin{pmatrix} h_\theta \\ h_r \end{pmatrix}, \tag{9}$$

where the $\pm$ sign depends on the polarization.

The case where $m' = 0$ reduces to two uncoupled equations:

$$\left(\frac{k^2}{r}\frac{d}{dr}\frac{r}{k^2}\frac{d}{dr} - \frac{1}{r^2} - \frac{g_r}{r} + k^2\right) h_\theta = \beta^2 h_\theta \tag{10}$$

for the Transverse Magnetic (TM) modes for which H_z is identically zero, and

$$\left(\frac{1}{r}\frac{d}{dr}r\frac{d}{dr}-\frac{1}{r^2}+k^2\right)h_r=\beta^2 h_r \tag{11}$$

for the Transverse Electric (TE) modes for which E_z is identically zero. Often, gradient index terms (those involving g_r) are neglected on the basis that profile variations are relatively small.[4] The difference or splitting in β^2 for the TM and TE modes measures the accuracy of this practice.

When $m' \neq 0$, eq. (9) is expressed as

$$\begin{pmatrix} A & B \\ B & A \end{pmatrix}\begin{pmatrix} h_\theta \\ h_r \end{pmatrix}+\frac{1}{2}\begin{pmatrix} a & b \\ -b & -a \end{pmatrix}\begin{pmatrix} h_\theta \\ h_r \end{pmatrix}=\beta^2\begin{pmatrix} h_\theta \\ h_r \end{pmatrix}, \tag{12}$$

where

$$A=\frac{1}{4}\frac{d}{dr}r\frac{d}{dr}-\frac{m'^2+1}{r^2}+k^2+\frac{a}{2}, \qquad a=-\frac{g_r}{r}\frac{d}{dr}r$$

$$B=\pm\frac{2m'}{r^2}+\frac{b}{2}, \qquad b=\pm\frac{m'g_r}{r}. \tag{13}$$

The initial term has eigenvectors of the form,

$$\begin{pmatrix} f_1 \\ f_1 \end{pmatrix}, \tag{14}$$

where $(A+B)f_1=\beta^2 f_1$, and

$$\begin{pmatrix} f_2 \\ -f_2 \end{pmatrix}, \tag{15}$$

where $(A-B)f_2=\beta^2 f_2$. The second term of eq. (12) is neglected because its first order perturbation contribution is zero, as in general

$$\begin{pmatrix} a & b \\ -b & -a \end{pmatrix}\begin{pmatrix} f \\ \pm f \end{pmatrix} \text{ is orthogonal to } \begin{pmatrix} f \\ \pm f \end{pmatrix}, \tag{16}$$

respectively. If two eigenvalues are equal or nearly equal, a degenerate-perturbation calculation may be required.

To first order, the modes when $m' \neq 0$ are either the $EH_{m',n}$ with transverse H fields of the form

$$H_{ot}=\begin{pmatrix} f\sin m'\theta \\ f\cos m'\theta \end{pmatrix} \text{ and } \begin{pmatrix} f\cos m'\theta \\ -f\sin m'\theta \end{pmatrix}, \tag{17}$$

where by eqs. (14) and (15) f satisfies

$$\left(\frac{k}{r}\frac{d}{dr}\frac{r}{k}\frac{d}{dr} - \frac{(m'+1)^2}{r^2} - \frac{(m'+1)}{2r}g_r + k^2\right)f = \beta^2 f, \tag{18}$$

or the $HE_{m',n}$ with

$$H_{ot} = \begin{pmatrix} f\cos m'\theta \\ f\sin m'\theta \end{pmatrix} \text{ and } \begin{pmatrix} f\sin m'\theta \\ -f\cos m'\theta \end{pmatrix}, \tag{19}$$

where f satisfies

$$\left(\frac{k}{r}\frac{d}{dr}\frac{r}{k}\frac{d}{dr} - \frac{(m'-1)^2}{r^2} + \frac{(m'-1)}{2r}g_r + k^2\right)f = \beta^2 f. \tag{20}$$

With $m = m' \pm 1$, eqs. (18) and (20) can be combined as

$$\left(\frac{k}{r}\frac{d}{dr}\frac{r}{k}\frac{d}{dr} - \frac{m^2}{r^2} \mp \frac{m}{2r}g_r + k^2\right)f = \beta^2 f. \tag{21}$$

The modes are indexed by the angular parameter m. For $m = 0$ there are two polarizations for each HE_{1n} mode. This group includes the fundamental mode HE_{11}, which propagates in single-mode fibers. For $m = 1$ there are two polarizations for the HE_{2n} modes, also the TM modes and the TE modes. For $m > 1$ there are two polarizations for the $HE_{m+1,n}$ modes and two for the $EH_{m-1,n}$ modes.

When gradient index terms are neglected, eq. (9) reduces to the scalar wave equation

$$\left(\frac{1}{r}\frac{d}{dr}r\frac{d}{dr} - \frac{m^2}{r^2} + k^2\right)f = \beta^2 f. \tag{22}$$

For $m = 0$ each solution represents two polarizations, i.e., two modes; for $m \neq 0$ each solution represents two polarizations and two angular harmonics, $m' = m \pm 1$, i.e., four modes.

The scalar wave equation and its counterparts [eqs. (10) and (21)] assume the form of a time-independent Schroedinger equation in two dimensions. In particular, the scalar wave equation can be expressed as

$$\left(\frac{1}{r}\frac{d}{dr}r\frac{d}{dr} - \frac{m^2}{r^2} + (k^2 - k_{cl}^2)\right)f = (\beta^2 - k_{cl}^2)f, \tag{23}$$

where

$$k_{cl} = 2\pi n_{cl}/\lambda. \tag{24}$$

The quantity $(k^2 - k_{cl}^2)$ plays the role of a potential that is 0 in the outer cladding and beyond; $(\beta^2 - k_{cl}^2)$ is an eigenvalue.

Results on Schroedinger's operators[23] imply that the propagation

modes correspond on a one-to-one basis to the positive eigenvalues and the number of such modes is finite (see Ref. 23, p. 366). This fact implies that increasingly accurate estimates of the propagation modes can be obtained by ever finer discretization of the equations. By contrast, finer discretizations introduce ever more negative eigenvalues corresponding to the continuum of radiation or unbound modes.

2.2 Finite element reduction

The Finite Element Method (FEM) can solve to desired accuracy the differential equations just derived. The present discussion specializes to the scalar wave equation [eq. (23)]; modifications needed for the equations containing gradient index terms are indicated in the appendix.

The solution function $f(r)$ is approximated by a piecewise linear function. This can be expressed in terms of interpolation functions (shown in Fig. 2) as

$$f(r) \cong \sum_{l=0}^{L+1} f(r_l) N_l(r), \tag{25}$$

where $r_l = l\delta$ for $l = 0, 1, \cdots, L+1$ are evenly spaced sample points.

The first and last terms of the series are affected by end conditions on $f(r)$. At the center ($r = 0$) of the fiber $f(r)$ and its radial derivative must be bounded and well defined; so $f(0) = 0$ when $m > 0$ and df/dr $(0) = 0$ or equivalently $f(0) = f(\delta)$ to first order in δ when $m = 0$.

At the other end, $R = L\delta$ represents a truncation radius in the cladding, and $R + \delta$ represents the truncated part in a way that will now be explained. Assuming that the cladding extends indefinitely, the solution there is

$$f(r) = aK_m(\eta r), \tag{26}$$

where K_m denotes the mth order modified Bessel function of the second kind,[24] a is an unknown coefficient,

$$\eta = (\beta^2 - k_{\text{cl}}^2)^{1/2}, \tag{27}$$

and m denotes the azimuthal mode number used in the scalar wave

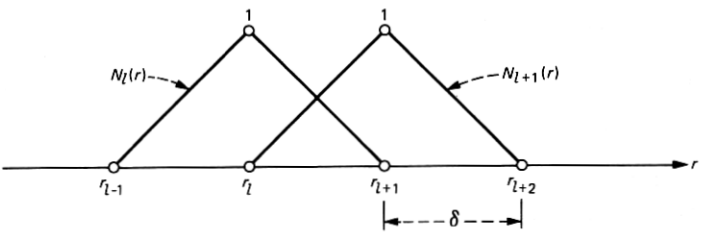

Fig. 2—Linear interpolation functions: hat functions.

equation [see eq. (23)]. It follows that the end condition for f at truncation is

$$f'/f = \eta K_m'(\eta R)/K_m(\eta R). \tag{28}$$

A Taylor's expansion of f to first order about $r = R$ yields

$$\begin{aligned} f(R + \delta) &= f(R) + \delta f'(R) \\ &= f(R)(1 + \delta\eta K_m'(\eta R)/K_m(\eta R)). \end{aligned} \tag{29}$$

Most modes of a multimode fiber are unaffected by the end condition in eq. (29) because their waveforms are negligibly small beyond the core. But the waveform of a single-mode fiber can extend beyond the core and then the end condition needs to be enforced.

Sample values of $f(r)$, the coefficients in eq. (25), are estimated by the Galerkin weighted residual method.[22] Although a piecewise linear approximation cannot satisfy the scalar wave equation, it can satisfy weighted averages of the equation. In the Galerkin technique the weightings are chosen as the basis functions $N_j(r)$ $j = 1, \cdots, L$. In terms of inner products, defined for any functions $p(r)$ and $q(r)$ as

$$(p, q) \equiv \int_o^{R+\delta} p(r)q(r)r\,dr, \tag{30}$$

Galerkin's technique yields

$$-\left(\frac{df}{dr}, \frac{dN_j}{dr}\right) - m^2\left(\frac{f}{r^2}, N_j\right) + \left((k^2 - k_{cl}^2)f, N_j\right) = (\beta^2 - k_{cl}^2)(f, N_j) \tag{31}$$

for $j = 1, \cdots, L$. The first term comes from an integration by parts.

Substituting the piecewise linear approximation of f [from eq. (25)] into the Galerkin equations gives L equations for $L + 2$ sample values, but the end conditions eliminate two of these values. The result is L equations in L unknowns, expressed as the matrix equation,

$$(A - m^2B + C)\mathbf{f} = \delta^2(\beta^2 - k_{cl}^2)D\mathbf{f}. \tag{32}$$

The column vector $\mathbf{f}$ denotes the sample values,

$$\mathbf{f} = [f(r_1), \cdots, f(r_L)]^t. \tag{33}$$

The $L \times L$ matrix A has jl element

$$a_{jl} = -\left(\frac{dN_l}{dr}, \frac{dN_j}{dr}\right)\delta^2 \tag{34}$$

for all j and l except, to accommodate the end conditions, a_{10} must be added to a_{11} when $m = 0$ and $a_{L,L+1}f_{L+1}/f_L$ must be added to a_{LL} for all

m. The $L \times L$ matrices B, C, and D have jl elements

$$b_{jl} = \left(\frac{1}{r^2} N_l, N_j\right) \delta^2,$$

$$c_{jl} = ((k - k_{\text{cl}}^2)N_l, N_j)\delta^2, \tag{35}$$

and

$$d_{jl} = (N_l, N_j).$$

The latter three matrices are evaluated by "lumping the masses," meaning that the integrals are evaluated numerically and the integration points are chosen as the sample points.[25] The trapezoidal rule then yields 0 for the off-diagonal elements and for the main diagonal gives

$$b_{ll} = \delta^2/l \; c_{ll} = l[k^2(r_l) - k_{\text{cl}}^2]\delta^4 \; d_{ll} = l\delta^2 \tag{36}$$

for $l = 1, \cdots, L$. The matrix A can be evaluated exactly. It is symmetric and tridiagonal (i.e., $a_{jl} = 0$ if $|l - j| > 1$) and has

$$a_{ll} = -2l\delta^2 \; a_{l,l+1} = (l + \tfrac{1}{2})\delta^2 \tag{37}$$

for $l = 1, \cdots, L$. When $m = 0$, a_{11} is $-1.5\delta^2$.

Eq. (32) converts to a standard symmetric eigenvalue problem by multiplying both sides by the diagonal matrix $D^{-1/2}$ and putting

$$\mathbf{g} = D^{1/2}\overline{\mathbf{f}}. \tag{38}$$

The result is

$$T\mathbf{g} \equiv D^{-1/2}(A - m^2B + C)D^{-1/2}\mathbf{g} = \delta^2(\beta^2 - k_{\text{cl}}^2)\mathbf{g}, \tag{39}$$

standard form relative to the vector $\mathbf{g}$.

The key matrix, T, is symmetric and tridiagonal. For $m \neq 0$

$$t_{ll} = -2 - \frac{m^2}{l^2} + \delta^2[k^2(r_l) - k_{\text{cl}}^2]$$

$$t_{l+1,l} = t_{l,l+1} = \frac{1}{2}\left[\left(\frac{l+1}{l}\right)^{1/2} + \left(\frac{l}{l+1}\right)^{1/2}\right] \tag{40}$$

for $l = 1, \cdots, L - 1$; for $m = 0$

$$t_{11} = -\tfrac{3}{2} + \delta^2[k^2(r_l) - k_{\text{cl}}^2]; \tag{41}$$

for all m

$$t_{LL} = -2 - \frac{m^2}{L^2} + \delta^2[k^2(r_L) - k_{\text{cl}}^2] + t_{L,L+1}g_{L+1}/g_L. \tag{42}$$

The end condition in eq. (29) combined with eq. (38) gives

$$g_{L+1}/g_L = \frac{L+1}{L}\,[1 + \delta\eta K_m'(\eta R)/K_m(\eta R)]. \tag{43}$$

Equation (39) represents the FEM reduction of the scalar wave equation. The other differential equations, as indicated in the appendix, reduce to the same form, with T symmetric and tridiagonal. The sample distance δ is discussed in Section III.

2.3 Calculation of the propagation modes

The propagation modes are calculated by solving for the positive eigenvalues (μ) of T. The associated propagation constants are

$$\beta = (\mu/\delta^2 + k_{\text{cl}}^2)^{1/2} \tag{44}$$

with effective index of refraction

$$n_e = \beta/(2\pi/\lambda) = \beta(c/\omega). \tag{45}$$

When the end condition is enforced, the T matrix depends on β in its (L, L) entry, but a simple iteration procedure yields the proper β. The associated waveforms are given by $\mathbf{f}$ or $\mathbf{g}$.

The modal delays per unit length (τ_g) are the reciprocal of the group velocities,

$$\tau_g = \frac{d\beta}{d\omega}. \tag{46}$$

An efficient calculation of these uses the formula,

$$\frac{d\beta}{d\omega} = \left(\frac{\omega}{\beta}\right)\left(\frac{d\beta^2}{d\omega^2}\right) = \left(\frac{c}{n_e}\right)\left[\frac{dk_{\text{cl}}}{d\omega^2} + \frac{1}{\delta^2}\left(\frac{dT}{d\omega^2}\,\mathbf{g}\right)\cdot\mathbf{g}\right], \tag{47}$$

where $\mathbf{g}$ is assumed to be normalized (i.e., $\mathbf{g}\cdot\mathbf{g} = 1$). This follows standard procedure for taking the derivative of an eigenvalue with respect to a parameter.[26] Equations (40), (41), and (42) for T imply that $dT/d\omega^2$ is a diagonal matrix. Using the equivalence between $\omega^2 d/d\omega^2$ and $-\lambda 2d/d\lambda^2$, eq. (47) becomes

$$\tau_g = \sum_{l=1}^{L}\left[n^2(r_l) - \lambda^2\,\frac{dn^2}{d\lambda^2}\,(r_l)\right] g_l^2/cn_e. \tag{48}$$

To form the T matrix, the index profile $n(r)$ must be available for any excitation wavelength (λ). Sellmeier expansions[27] of the form

$$n^2 = 1 + \sum_{i=1}^{3} A_i/[1 - (l_i/\lambda)^2] \tag{49}$$

have been fitted to measured values of refractive index over the range of wavelengths 0.8 μm to 1.5 μm for bulk samples of pure SiO_2, 13.5-percent Ge doped SiO_2, and 1 percent F doped SiO_2 (denoted here as

a, b, and c, respectively). Also, results in Ref. 28 indicate that the index is approximately linear with concentration. Therefore, the index profile of an optical fiber having a graded Ge dopant is taken as

$$n(r, \lambda) = a(\lambda) + C_n(r)[b(\lambda) - a(\lambda)], \tag{50}$$

where $C_n(r)$ denotes the concentration profile for Ge, relative to 13.5 percent. For dual dopants, Ge and F, the index profile is

$$n(r, \lambda) = a(\lambda) + C_n(r)[b(\lambda) - a(\lambda)] + \tilde{C}_n(r)[c(\lambda) - a(\lambda)], \tag{51}$$

where $\tilde{C}_n(r)$ denotes the concentration profile for F, relative to 1 percent.

The concentration profiles in these equations may be specified or may be deduced from the index profile at a reference wavelength. Once the concentration profiles are available, the index profile and its λ^2 derivative can be determined from eq. (50) or eq. (51) for any wavelength.

The T matrix can be expressed in dimensionless form by replacing the sample spacing by

$$\delta = R_1/L_1, \tag{52}$$

where R_1 denotes the core radius and L_1 the number of samples in the core. This gives

$$\delta^2[k^2(r) - k_{\text{cl}}^2] = (2\pi R_1/\lambda)^2(n^2(r) - n_{\text{cl}}^2)/L_1^2, \tag{53}$$

and from eq. (50), (with $a = n_{\text{cl}}$),

$$n^2(r) - n_{\text{cl}}^2 = C_n(n_1^2 - n_{\text{cl}}^2) + (C_n^2 - C_n)(n_1 - n_{\text{cl}})^2, \tag{54}$$

where now $C_n(r)$ represents the Ge concentration normalized with respect to n_1, the index at the center. The latter term in eq. (54) can usually be neglected because $n_1 \sim n_{\text{cl}}$ and often, $C_n(r) \sim 1$ for most r. Then the T matrix can be expressed in terms of the usual V number,

$$V = (2\pi R_1/\lambda)(n_1^2 - n_{\text{cl}}^2)^{1/2} = R_1(k_1^2 - k_{\text{cl}}^2)^{1/2} \tag{55}$$

and the effective V number,

$$V_e = (2\pi R_1/\lambda)(n_e^2 - n_{\text{cl}}^2)^{1/2} = R_1(\beta^2 - k_{\text{cl}}^2)^{1/2} \tag{56}$$

for the (L, L) element. The FEM reduction becomes

$$T(V, V_e)\mathbf{g} = (V_e/L_1)^2\mathbf{g}, \tag{57}$$

where now an iteration on V_e is required. A similar expression, involving three V numbers, holds for dual dopants.

The effective index (n_e) is obtained from V_e in eq. (56). The delay

is

$$\tau_g = \frac{\omega}{\beta}\frac{d\beta^2}{d\omega^2} = \frac{1}{R_1^2}\frac{dV_e 2}{dV^2}\frac{dV^2}{d\omega^2} + \frac{dk_{\mathrm{cl}}^2}{d\omega^2}$$

$$= \frac{1}{cn_e}\left\{n_{\mathrm{cl}}^2 - \lambda^2\frac{dn_{\mathrm{cl}}^2}{d\lambda^2} + \frac{V_e}{V}\frac{dV_e}{V}\right.$$

$$\left.\cdot\left[(n_1^2 - n_{\mathrm{cl}}^2) - \lambda^2\frac{d}{d\lambda^2}(n_1^2 - n_{\mathrm{cl}}^2)\right]\right\}. \tag{58}$$

Matrix T is always symmetric and tridiagonal. The routine BISECT in the EISPACK[1] library computes the positive eigenvalues for such matrices and TINVIT, also in EISPACK, computes the associated eigenvectors **g**. These routines operate efficiently and reliably.

2.4 Leaky modes

When the index profile drops below n_{cl} over part of its range, then leaky modes may exist. These modes have $n_e < n_{\mathrm{cl}}$ and complex propagation constants. The corresponding attenuation accounts for radiation loss as the waveform spreads out radially. As is well known, leaky modes also can arise when $m \neq 0$ from the negative term, $-(m^2/r^2)$, in the propagation equation.

Leakage loss is calculated by truncating the waveform at the beginning of the outer cladding and enforcing the proper end condition. In terms of the complex propagation constant γ, eq. (27) for η changes to

$$\eta = (-\gamma^2 - k_{\mathrm{cl}}^2)^{1/2}, \tag{59}$$

and the end condition [in eq. (43)] becomes complex. Now, the T matrix has a real (T_r) and an imaginary (T_I) part, but matrix T_I consists of all zeroes except the (L, L) diagonal element (call it x). First-order perturbation theory estimates an eigenvalue of T as

$$\mu = \mu_r + ixg_L^2 = \delta^2\eta^2, \tag{60}$$

where μ_r is an eigenvalue of T_r and g_L is the Lth component of the associated normalized eigenvector **g**. Again, an iteration is required because T depends on γ.

III. EXAMPLES OF MODAL CALCULATIONS

In this section modal calculations based on the results of Section II are illustrated in 10 examples. The next section summarizes and evaluates the results.

3.1 Infinite parabolic profile

The parabolic profile that extends without radial limit has index

$$n(r) = n_1[1 - 2\Delta(r/R)^2]^{1/2} \tag{61}$$

for all r, where R denotes the nominal radius of the fiber core. Under the scalar wave approximation, its modal waveforms are Laguerre Gaussian functions, its propagation constants are

$$\beta_{\mu m} = [k_{cl}^2 n_1^2 - 2Qk_{cl}n_1(2\Delta)^{1/2}/R]^{1/2}, \tag{62}$$

and its modal delays (neglecting material dispersion) are

$$\tau_{\mu m} = (\beta_{\mu m} + k_{cl}^2 n_1^2/\beta_{\mu m})/2\omega, \tag{63}$$

where the mode number is

$$Q = 2\mu + m + 1 \qquad m, \mu = 0, 1, \cdots, \tag{64}$$

with m the angular harmonic and μ the radial harmonic. Each Q represents a group of modes that have the same propagation constant and delay (see Ref. 9).

Modal delays were calculated assuming parameter values $\Delta = 0.013$, $R = 25$ μm, and $\lambda = 1.3$ μm. Convergence with respect to truncation radius (TR) was complete (within 0.1 ps/km) for each mode for $TR = 1.5R$. Convergence with respect to the number (L_1) of sample points in the core was within 1 ps/km in the rms delay for $L_1 = 400$, as indicated in Table I. An accuracy of 1 ps/km determines the bandwidth within 5 percent for a 10-GHz × km fiber and 0.5 percent for a 1-GHz × km fiber. The percent errors of the computed delays (with $L_1 = 500$) are shown in Fig. 3.

The most accurately computed mode within a mode group had radial number $\mu = 0$; their waveforms have no zero-crossings and are most easily approximated by piecewise linear functions. The least accurately computed mode (which was off by 5.5 ps/km) had the largest μ. As another measure of accuracy, the spread in the computed delays for each Q is also given in Table I.

To test the single-mode case, the parameters were changed to $\Delta =$

Table I—Convergence results for infinite parabolic profile in units of ps/km*

L_1	τ_{RMS}	Spread (1)	Spread (2)
100	144.0	136.1	96.5
200	129.4	33.9	23.7
300	127.1	15.1	10.5
400	126.3	8.5	5.9
500	125.9	5.5	3.8

* ($\Delta = 0.013$, $R = 25$ μm, $\lambda = 1.3$ μm)

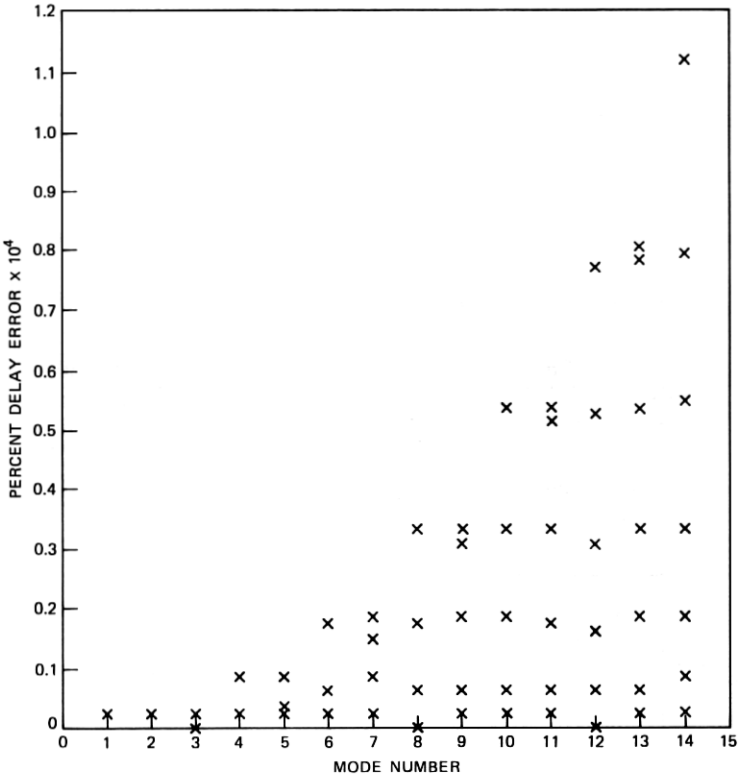

Fig. 3—Computation errors in modal delays for infinite parabolic profile.

0.005 and $R = 5$ μm, but again $\lambda = 1.3$ μm. The calculated effective index of the HE_{11} mode was accurate to seven decimal places and the delay to 0.1 ps/km when TR was $2.5R$ and L_1 was 300. This precision translates to nm accuracy in the zero-dispersion wavelength. The beam radius (BR) defined by the condition

$$f^2(BR) = f^2(0)/e \tag{65}$$

was accurate to four decimal places, as indicated in Table II. The number of samples in the core can be less in the single-mode case because the HE_{11} waveform does not oscillate; the truncation radius needs to be greater because the waveform extends farther into the cladding.

3.2 Parabolic fiber

Power-law fibers have the index profile

$$n(r) = \begin{cases} n_1(1 - 2\Delta(r/R)^{\alpha})^{1/2} & r \le R \\ n_1(1 - 2\Delta)^{1/2} & r \ge R. \end{cases} \tag{66}$$

Assuming parameter values of $\Delta = 0.013$, $R = 25$ μm, $\lambda = 1.3$ μm, and $\alpha = 2$ (the parabolic case), effective index (n_e) and delay (τ_g) were computed for each propagation mode under the scalar wave approximation. The rms delay (τ_{RMS}) converged to 1.793 ns/km within 0.3 percent and the rms delay with the two highest-order-mode groups deleted (τ'_{RMS}) converged to 113 ps/km within 0.9 percent when $L_1 = 300$ and $TR = 0.7R$.

Figure 4 shows n_e and τ_g for each mode arranged by mode group.

Table II—Modal quantities for HE_{11} mode of parabolic profile*

L_1	TR	n_e	τ_g (μs/km)	BR (μm)
300	$3R/2$	1.4531412	4.8581500	2.6561930
300	$2R$	1.4531608	4.8577058	2.6644067
400	$2R$	1.4531608	4.8577059	2.6644135
300	$5R/2$	1.4531609	4.8577024	2.6644397
Actual Values		1.4531609	4.8577025	2.6643516

* ($\Delta = 0.013$, $R = 25$ μm, $\lambda = 1.3$ μm)

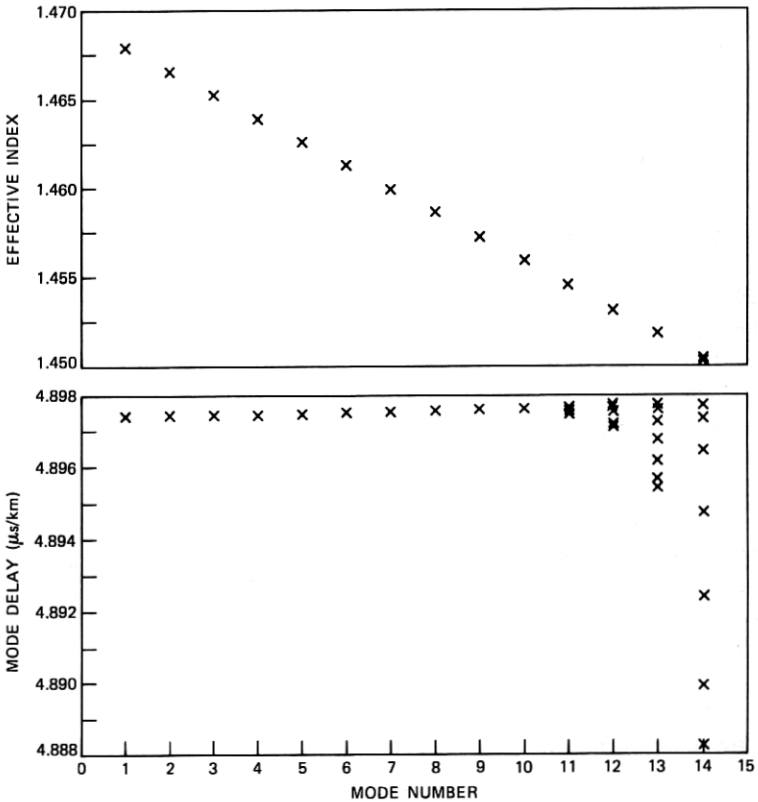

Fig. 4—Plots of n_e and τ_g versus mode number for parabolic fiber.

The delays spread almost 10 ns/km for $Q = 14$ and 3 ns/km for $Q = 13$, but less than 1 ns/km for the others. The spread in n_e is negligible, reaching a maximum of 0.01 percent.

Figure 5 shows n_e and τ_g plotted jointly on an expanded delay scale with outliers excised. To compare with WKB results, n_e and τ_g for the corresponding infinite parabola are indicated. The reference delays exceed all in their mode group: by as little as 0.2 ps/km for each of the first nine mode groups, but by more than 34 ps/km and 86 ps/km for $Q = 13$ and 14, respectively.

3.3 Contribution of gradient index terms

Gradient index terms cause modal delays to spread still further. Figure 6 shows the delay differences caused by these terms for each mode of the parabolic fiber. Of the 112 modal delays only 14 differed by more than 20 ps/km from the corresponding scalar wave values. The TM mode nearest cutoff had the largest difference (33 ps/km).

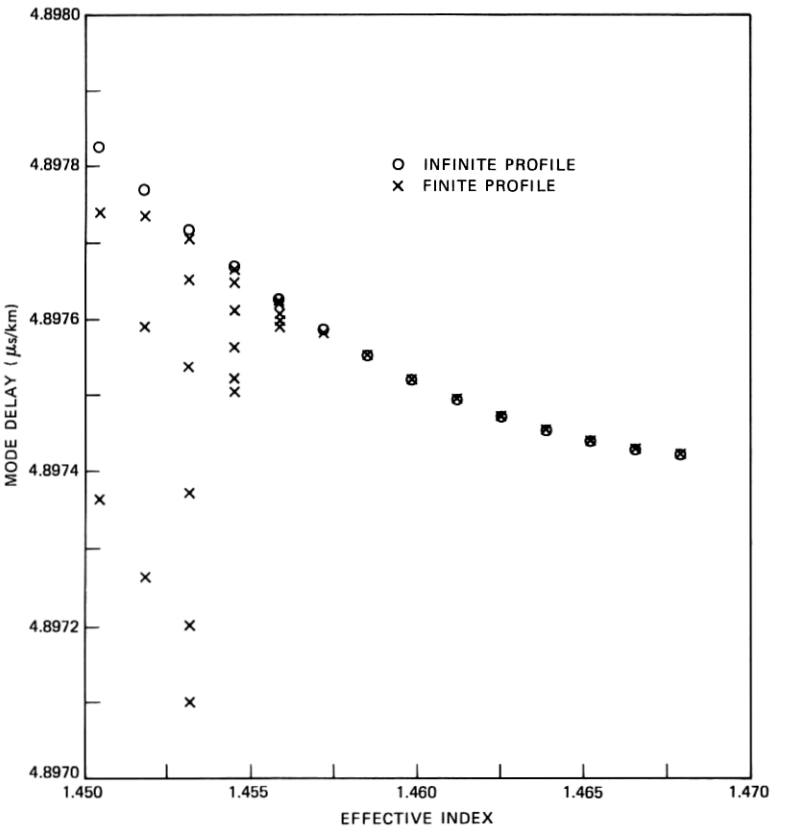

Fig. 5—Plots of τ_g versus n_e for cladded and infinite parabolic profiles.

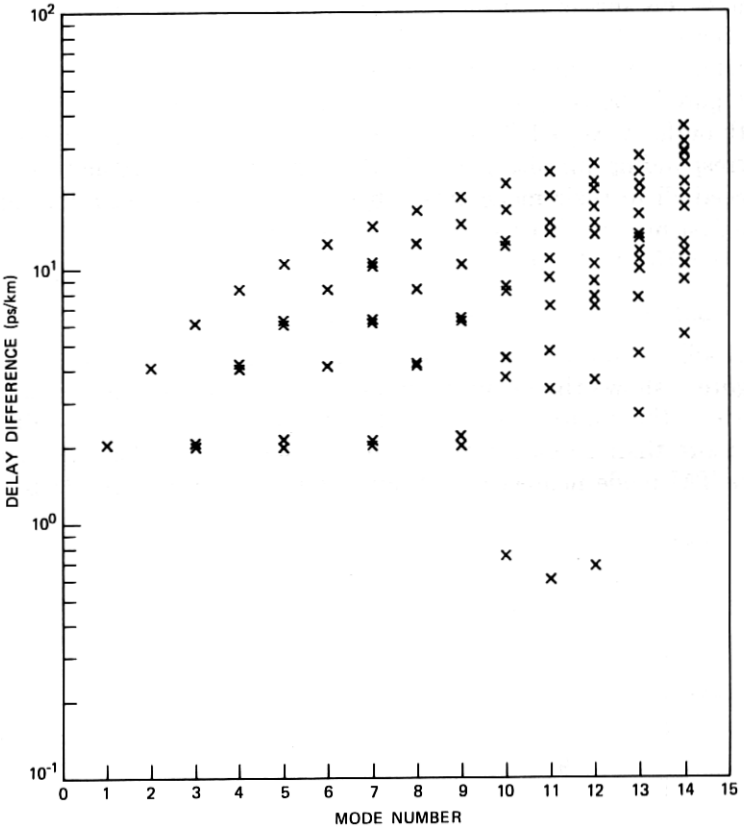

Fig. 6—Absolute differences in modal delays due to gradient index terms for parabolic fiber.

The change in τ_{RMS} was 5.9 ps/km and in τ'_{RMS} it was less than 1.5 ps/km. The error is less than 1.5 percent in either case. In the examples that follow gradient index terms are neglected.

3.4 Bandwidth of the parabolic fiber vs. λ

Material dispersion causes the bandwidth of power-law fibers to depend sharply on the excitation wavelength (λ). Here and in the following examples, the profile is assumed known at the reference wavelength of $\lambda = 0.8$ μm; the concentration profile and the index profile at other wavelengths are determined, as discussed in the previous section.

Bandwidth is defined as the half-power frequency of the transfer function over some distance. When intramodal dispersion is neglected, the transfer function is

$$G(\omega) = \sum_n a_n \exp(i\omega\tau_n), \tag{67}$$

where τ_n denotes the delay and a_n^2 the power of the nth mode. Defining the rms delay (τ_{RMS}) by

$$\tau_{\mathrm{RMS}} = \left[\sum_n a_n(\tau_n - \tau_{\mathrm{av}})^2 \Big/ \sum_n a_n\right]^{1/2} \tag{68}$$

and the average delay by

$$\tau_{\mathrm{av}} = \sum_n a_n\tau_n \Big/ \sum_n a_n, \tag{69}$$

then to second order in the $\omega(\tau_n - \tau_{\mathrm{av}})$, the bandwidth is

$$BW = 1/(2\pi\tau_{\mathrm{RMS}}), \tag{70}$$

in units of GHz × km for delays in ns/km.

Bandwidth was calculated on this basis over a range of wavelengths for the parabolic fiber of example 2, assuming the tapered modal-power distribution shown in Fig. 7. Lower-order modes are weighted more heavily than the higher and the highest are omitted as the higher modes are increasingly vulnerable to microbending and cladding absorption.

Figure 8 shows the spectral plot of bandwidth. The peak value occurs at $\lambda \simeq 0.963$ μm, compared to 0.983 μm reported in Ref. 13.

The spectral plot is also shown for the case where material dispersion is neglected. The figure shows that the bandwidth is lower and essen-

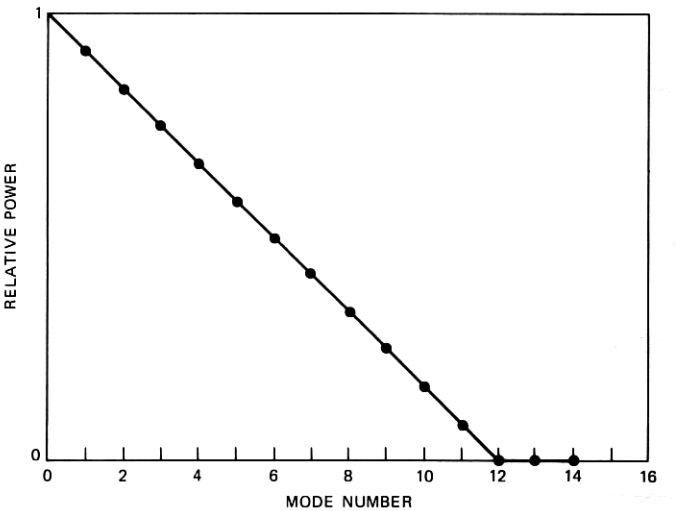

Fig. 7—A plot of the tapered modal-power distribution.

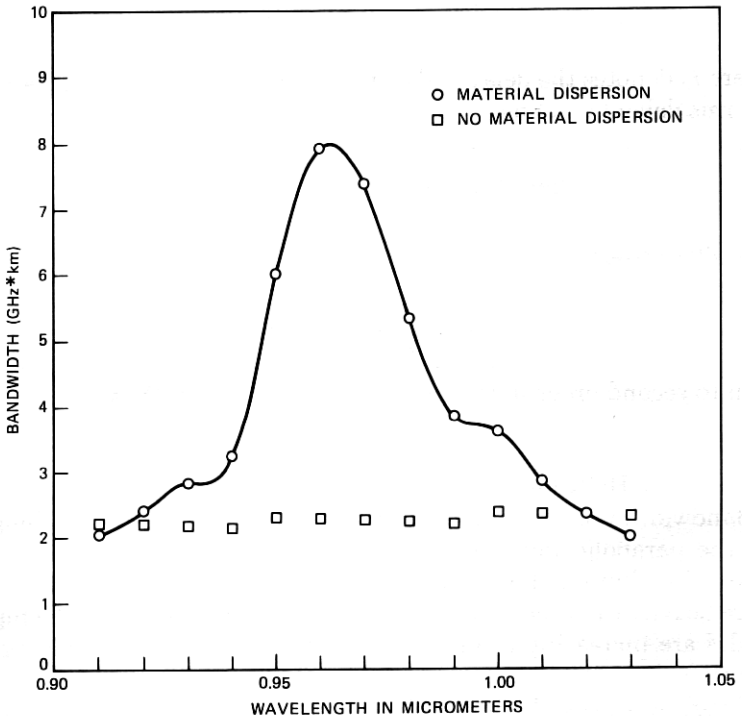

Fig. 8—Plots of bandwidth versus wavelength for parabolic fiber with and without material dispersion, using tapered modal-power distribution.

tially constant except for small discontinuities associated with new modes cutting in. Other calculation indicates that bandwidth increases to a peak at 9.5 GHz × km for $\alpha \simeq 1.98$ compared to an optimum $\alpha \simeq 1.97$ estimated by WKB analysis.[4]

3.5 Optimum α for power-law fibers

Material dispersion causes the optimum α of power-law fibers to depend on excitation wavelength. Figure 9 shows bandwidth versus α when $\Delta = 0.013$ and $R = 25$ μm for $\lambda = 0.82$ μm and $\lambda = 1.32$ μm. The optimum α's are 2.07 for the former and 1.88 for the latter, compared to values of 2.081 and 1.884, respectively, reported in Ref. 13. The peak bandwidths are 5.48 GHz × km and 6.02 GHz × km, respectively.

3.6 An alternate modal-power distribution

The fractional power that propagates in the cladding can be used to derive an alternate modal-power distribution. Modes with more than 0.1 percent of their power in the cladding will lose most of their power over 1 km for typical cladding losses of 1 dB/m. A realistic modal

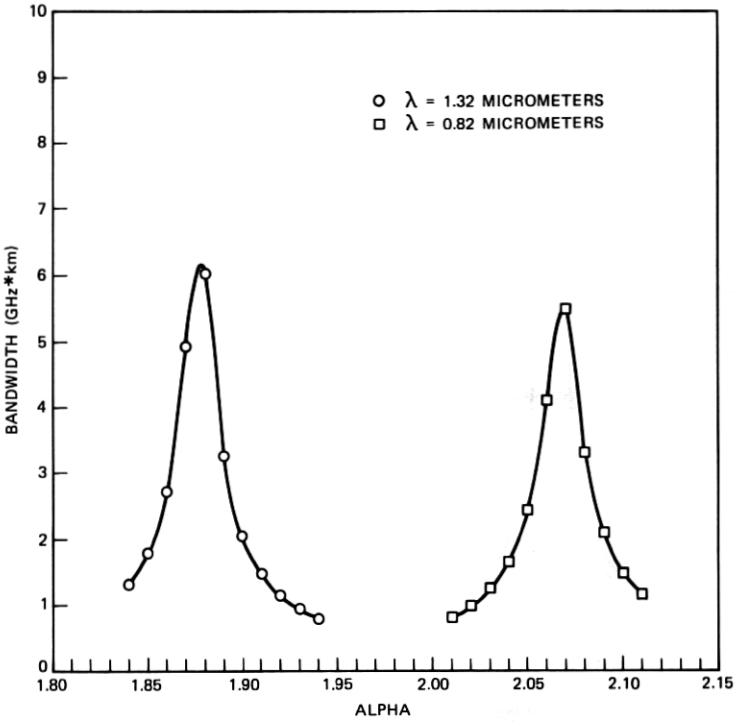

Fig. 9—Plots of bandwidth (in power-law fibers) versus α for $\lambda = .82$ μm and $\lambda = 1.32$ μm, using tapered modal-power distribution.

distribution would neglect these modes and for simplicity could weight the others equally.

Figure 10 shows bandwidth versus α for the two cases of example 5, assuming the new distribution. The optimum α is lower by 0.01 and the peak bandwidth is increased by 40 to 50 percent in either case. Table III indicates the modes neglected in the bandwidth calculation when $\lambda = 1.32$ μm and $\alpha = 1.88$.

3.7 Layer structure

Layer structure in actual fibers perturbs the ideal profile. In this example power-law profiles are approximated by steps that span equal areas and match the ideal profile at the mid-area points of the layers (see Fig. 11). Bandwidth at $\lambda = 1.32$ μm (using the modal distribution in example 6) is shown versus α and the number of steps (NS) in Fig. 12. The graphs indicate that the optimum α is essentially independent of NS, but the peak bandwidth and its sharpness decrease for smaller NS.

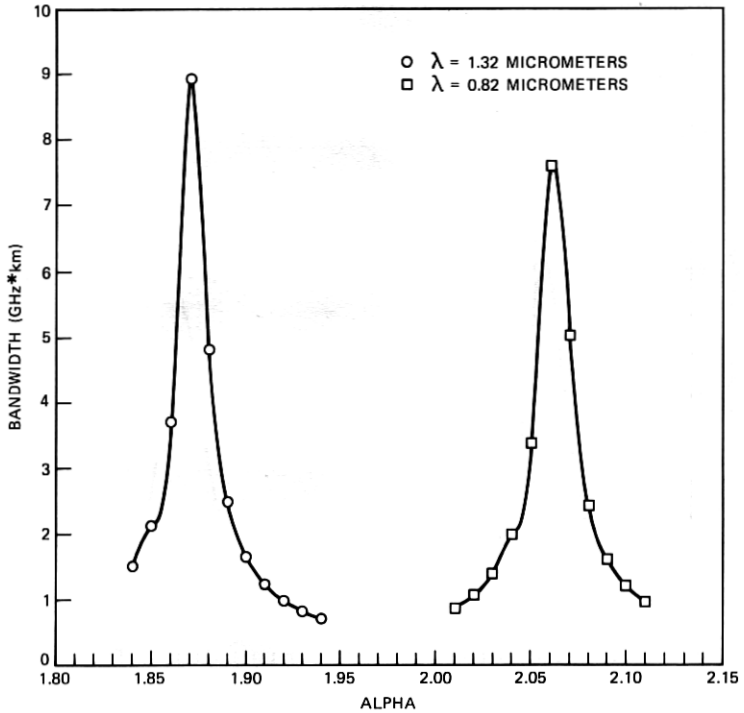

Fig. 10—Plots of bandwidth versus α for $\lambda = .82$ μm and $\lambda = 1.32$ μm assuming equal excitation of modes having less than 0.1 percent power in cladding.

3.8 Delay vs. λ for a single-mode fiber

Delay (per km) of the HE_{11} mode was computed versus λ for an actual single-mode fiber based on its measured index profile. The profile measurement was performed on the associated preform and is shown in Fig. 13. The depression of the inner cladding is due to F doping.

As the calculation presumes radially symmetric profiles, the right and left sides were considered separately. About 750 sample points were used in either case.

The radial scale of the fiber profile was assumed to depend linearly on that of the preform. The fiber core radius (R) was estimated from the preform core radius (RP), fiber diameter (DF), and preform diameter (DP) as

$$R = 1.01(RP)(DF/DP), \tag{71}$$

where the 1-percent addition estimates the SiO_2 loss in the outer cladding during the draw process.

Table III—Modes with less than 0.1 percent of their power in cladding*

	<0.1 Percent		>0.1 Percent	
Q	m	μ	m	μ
14	1	6		
	3	5		
13	0	6	12	0
	2	5		
	4	4		
	6	3		
	8	2		
	10	1		
12	1	5	11	0
	3	4		
	5	3		
	7	2		
	9	1		
11	0	5	8	1
	2	4	10	0
	4	3		
	6	2		
10	1	4	3	3
			5	2
			7	1
			9	0

* ($\Delta = 0.013$, $R = 25$ μm, $\lambda = 1.32$ μm, $\alpha = 1.88$)

Figure 14 shows computed differential delay versus λ for the right and left profiles together with measurements. It was assumed that measurement matched calculation exactly at $\lambda = 1.32$ μm, because only relative delays were measured. The zero-dispersion wavelength (at the delay minimum) was computed as $\lambda_o = 1.3127$ μm for the left profile and $\lambda_o = 1.3113$ μm for the right, compared to measurement of $\lambda_o = 1.3114$ μm.

3.9 Leakage loss vs. λ for a single-mode fiber

Leakage loss (in dB/m) of the TE mode of the single-mode fiber in the preceding example was calculated for both sides of the profile as a function of λ and is shown in Fig. 15. The difference between the left and right profiles becomes evident in this figure. A loss of 4 dB/m has been identified[29] with effective cutoff, and corresponds to cutoff wavelengths, $\lambda_c = 1.17$ μm for the left profile and $\lambda_c = 1.23$ μm for the right, compared to a measurement of 1.28 μm. This discrepancy is discussed in the next section.

The equivalent step approximation (where the index of the core and the inner cladding are area-weighted averages of the profile) gives $\lambda_o = 1.308$ μm and $\lambda_c = 1.21$ μm. The λ_c value straddles the previous calculated values, but the λ_o value is somewhat less.

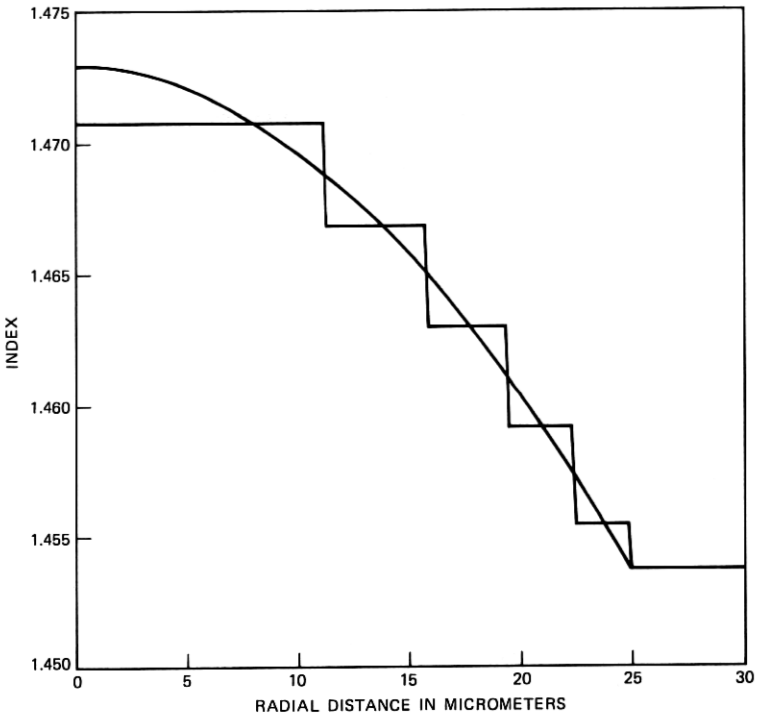

Fig. 11—A plot of a multilayered fit to an α profile (NS = 5, $\alpha = 1.90$).

3.10 Design curves for single-mode fibers

The dimensionless formulation allows design curves to be generated efficiently. Figure 16 shows V_e versus V for the HE_{11} mode of three power-law profiles. The specific parameters (R, Δ, λ) determine V and, hence, V_e and dV_e/dV. Delay versus λ is computed according to eq. (58) and λ_o is estimated at the minimum of the delay curve. Figure 17 shows λ_o versus R for two values of Δ for triangular profiles ($\alpha = 1$).

IV. SUMMARY AND CONCLUSIONS

A method for computing modes of a circular optical fiber has been presented. The finite element method reduces Maxwell's equations to the standard eigenvalue problem, involving tridiagonal matrices. Routines from EISPACK exploit the tridiagonal form to compute the eigenvalues and eigenvectors efficiently. From these the modal quantities are obtained.

Using a piecewise linear approximation of the waveform is necessary to get tridiagonal form. Although piecewise quadratic and cubic approximations of the waveform can lead to smaller matrices, tridiagonal

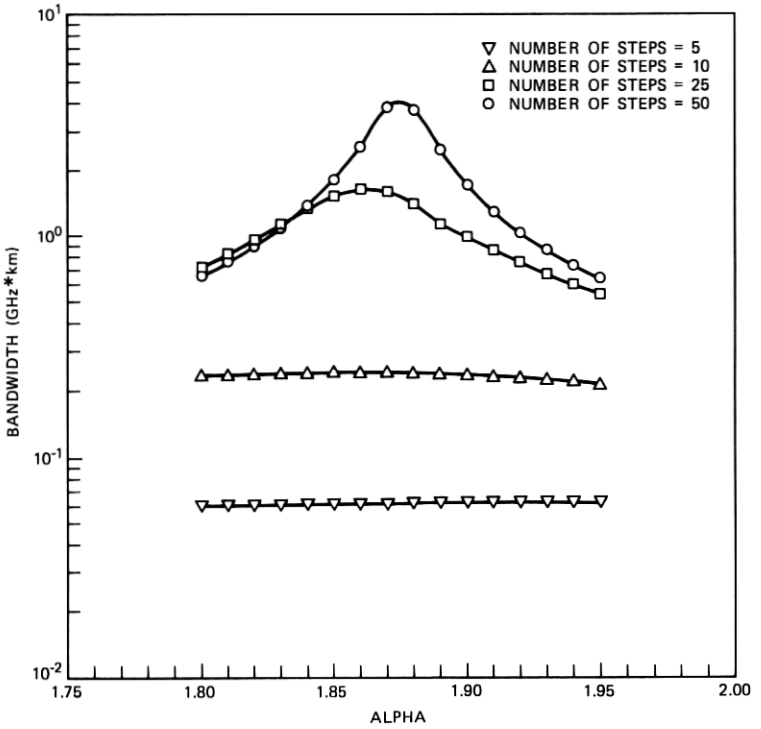

Fig. 12—Plots of bandwidth versus α at $\lambda = 1.32$ μm for four values of NS.

form is lost and the eigencalculations would be less efficient. Extension to elliptical and other nonradially symmetric fibers leads to similar difficulty in the eigen calculations.

The method applies to any circular fiber and can account for gradient index terms to first order. As illustrated in the 10 examples of Section III, the calculations can provide information on the radial distribution of propagating power, on pulse dispersion (arising from material, intermodal, and intramodal dispersion), and on leakage loss.

The accuracy of the method was tested for the infinite parabolic profile of the first example. After convergence was established, the modal quantities were compared with the actual values known through analysis. Agreement was excellent for both a multimode and a single-mode profile.

The WKB and scalar wave approximations were tested for the parabolic fiber in the next two examples. The cladding of the fiber altered the delays of the higher-order modes substantially, a facet missed by WKB analysis. The gradient index terms contributed less than 1.5 percent to the rms delay; and so, for most purposes the scalar wave approximation suffices for this fiber. The validity of these

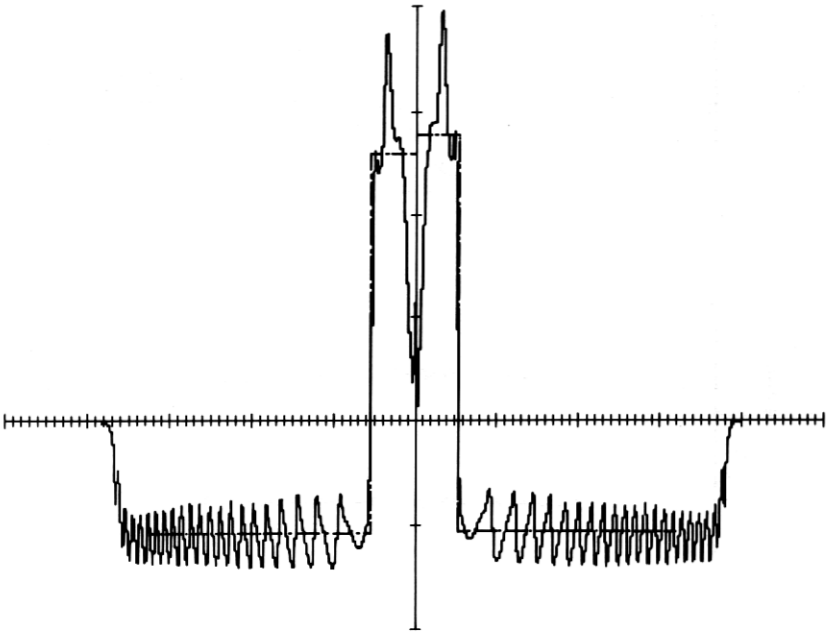

Fig. 13—The preform profile for a single-mode optical fiber.

approximations may change in other fibers; the value of the method is that it permits the test.

Material dispersion was incorporated into the calculation in the remaining examples. The variation of refractive index with wavelength and dopant concentration was modeled by Sellmeier expansions based on measurements of bulk samples with certain dopant concentration.[27] A linear dependence of index on concentration was assumed, but is not essential to the method. Irreversible thermal and stress effects[30] might also be incorporated.

Bandwidth was estimated in examples 4 and 5 for power-law fibers assuming a tapered modal-power distribution. With the higher-order mode groups deemphasized, results essentially agreed with WKB analysis. The usual sharp peak in bandwidth occurred in the spectral plot for the parabolic ($\alpha = 2$) fiber in example 4 and in the α-dependence in example 5. Calculation of optimum α agreed reasonably well in these cases with other numerical work and WKB calculations.

The bandwidth calculation was repeated in example 6 using a different modal-power distribution. Modes with more than 0.1 percent of their power in the cladding were neglected, as being too lossy to maintain power. The optimum α's were essentially the same, but peak

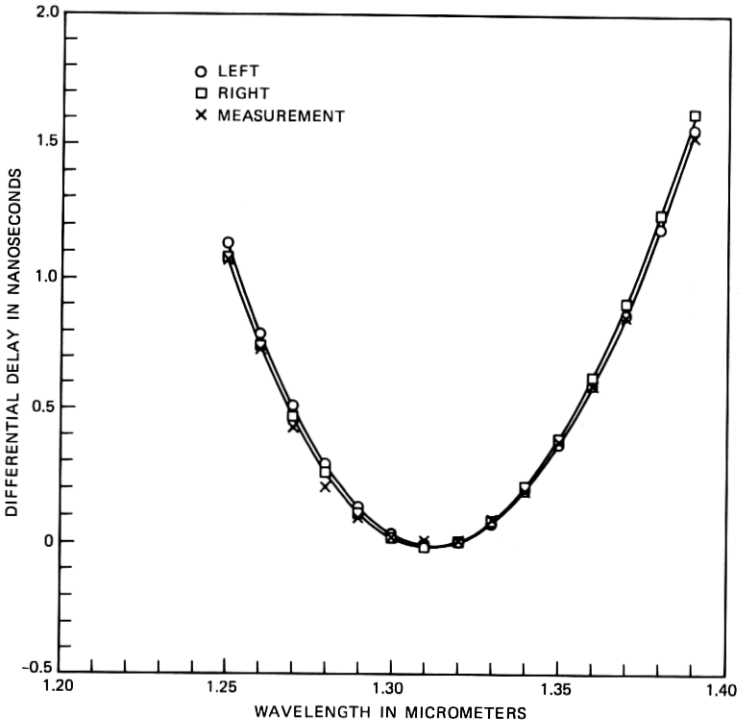

Fig. 14—Measurement and calculations for left and right profiles of differential delay versus wavelength.

bandwidths were somewhat higher. This example could be expanded to simulate differential mode attenuation, mode mixing, concatenation of dissimilar fibers, and other longitudinal variations.

Perturbations of α profiles usually lower bandwidth. Example 7 concerned the effect of layer structure on bandwidth and showed the expected decline with a smaller number of layers. Other perturbations such as ripple can also be treated. As a measure of its efficiency, the method used about two seconds per profile on the *Cray-1* for this example.

The last three examples concerned single-mode fibers. The first two of these involved an actual fiber whose profile was measured in the preform stage. Calculation of delay (per km) versus λ matched measurement extremely well, but calculated leakage loss exceeded measurement, giving a 7-percent average underestimate of cutoff wavelength (λ_c). Other calculations of leakage involving only slightly depressed inner claddings, where λ_c matches measurement to within 1 percent, suggest that the discrepancy may involve material changes in the F-doped glass caused by the draw process (consistent with obser-

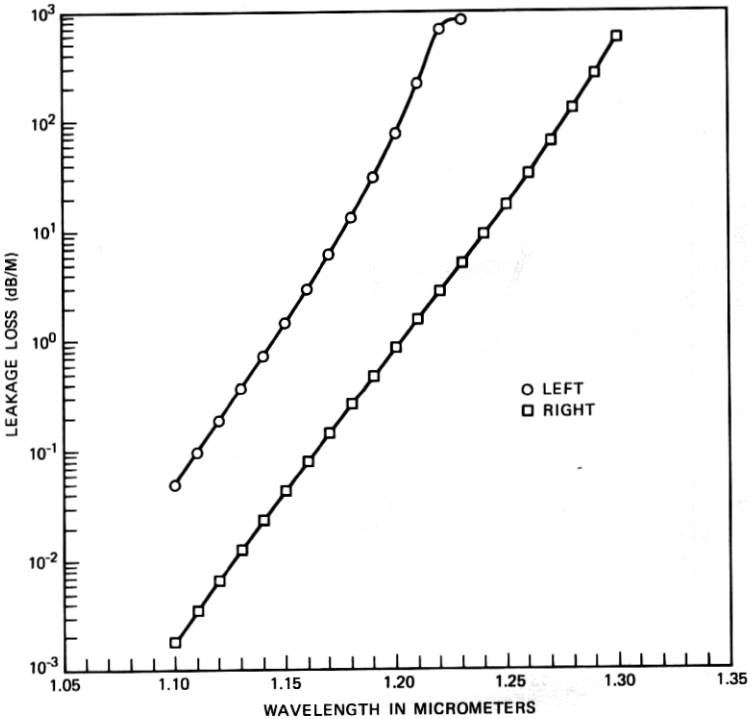

Fig. 15—Plots of computed leakage loss versus wavelength for left and right profiles.

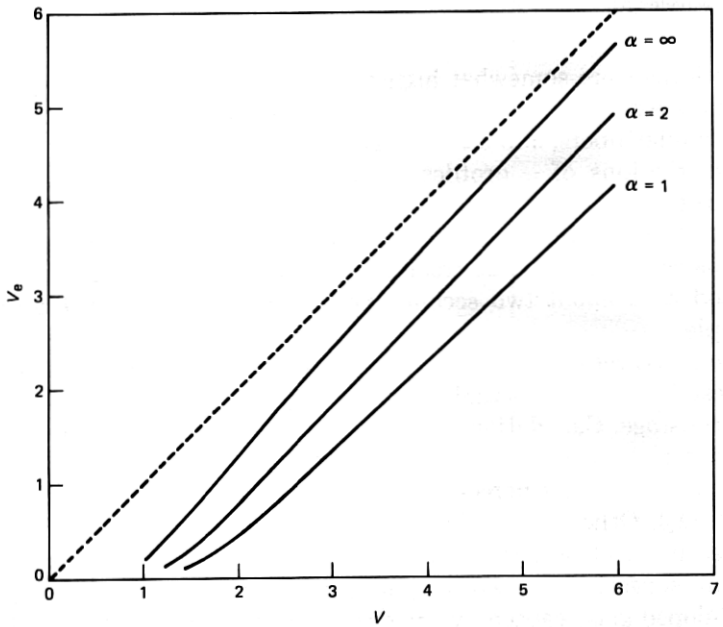

Fig. 16—Plots of V_e versus V for the HE_{11} mode of three power-law profiles.

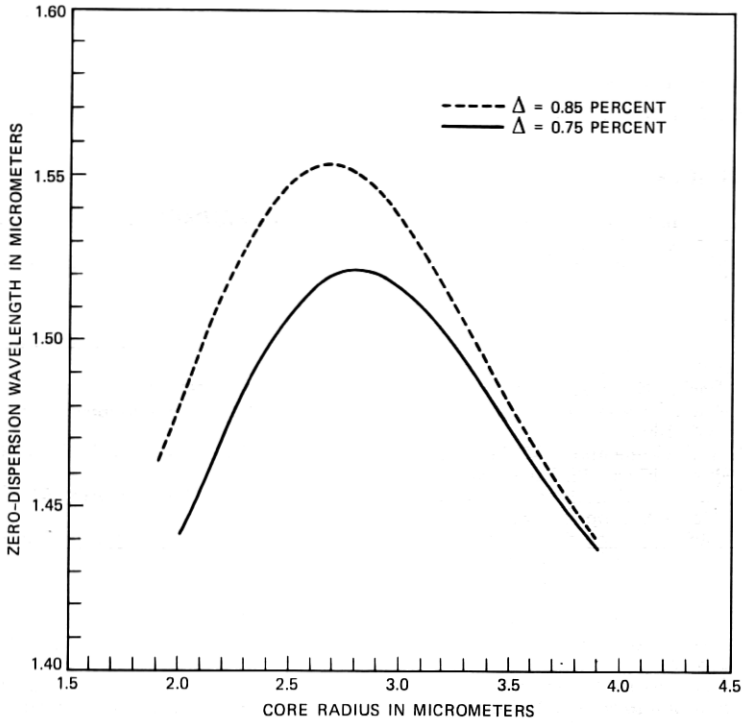

Fig. 17—Plots of computed zero-dispersion wavelength (λ_o) versus core radius (R) for two values of Δ, for triangular profiles.

vations in Ref. 31). Such changes need to be understood when predicting transmission performance from a preform profile. Similar values for λ_o and λ_c were obtained for the equivalent step profile (with depressed inner cladding), but the lower λ_o indicates the effect of profile structure.

The dimensionless formulation permits the greatest efficiency in getting design curves. Zero-dispersion wavelength (λ_o) for triangular profiles is calculated in example 10 showing the expected shift[32] to higher wavelengths. Spot size or cutoff wavelength can be obtained with similar efficiency.

In summary, the calculation method is reliable, and relatively inexpensive. In the context of circular fibers it is comprehensive, capable of simulating diverse effects.

V. ACKNOWLEDGMENTS

The author is grateful for useful discussions with I. A. White and A. J. Ritger on multimode fibers, W. T. Anderson and P. F. Glodis on

single-mode fibers, D. S. Burnett on the FEM, and L. Kaufman on EISPACK.

The author is also grateful to J. S. Nobles and D. L. Philen for fiber measurements and to H. W. Friedrichsen for programming support.

REFERENCES

1. B. T. Smith et al., *Matrix Eigensystem Routines—EISPACK Guide*, New York: Springer Verlag, 1976.
2. P. M. Morse and H. Feshback, *Methods of Theoretical Physics*, New York: McGraw-Hill, 1953, p. 1092.
3. J. E. Midwinter, *Optical Fibers for Transmission*, New York: Wiley, 1979, Chapter 6.
4. D. Gloge and E. A. J. Marcatili, "Multimode Theory of Graded-Core Fibers," B.S.T.J., *52*, No. 9 (November 1973), pp. 1563–78.
5. C. Pask, "Exact Expressions for Scalar Modal Eigenvalues and Group Delays in Power-Law Optical Fibers," J. Opt. Soc. Am., *69*, No. 11 (November 1979), pp. 1599–1603.
6. G. A. E. Crone and J. M. Arnold, "Anomalous Group Delay in Optical Fibers," Opt. Quant. Elect., *12*, No. 6 (November 1980), pp. 511–7.
7. E. Snitzer, "Cylindrical Dielectric Waveguide Modes," J. Opt. Soc. Am., *51*, No. 5 (May 1961), pp. 491–8.
8. S. Kawakami and S. Nishida, "Characteristics of a Doubly Clad Optical Fiber with a Low-Index Inner Cladding," IEEE Trans., *QE-11* (December 1974), pp. 879–87.
9. D. Marcuse, *Light Transmission Optics*, New York: Van Nostrand, 1972, pp. 267–72.
10. R. A. Sammut and A. K. Ghatak, "Perturbation Theory of Optical Fibers with Power-Law Core Profile," Opt. Quant. Elect., *10*, No. 6, (November 1978), pp. 475–82.
11. G. E. Peterson, A. Carnevale, U. C. Paek, and D. W. Berreman, "An Exact Numerical Solution to Maxwell's Equations for Lightguides," B.S.T.J., *59*, No. 7 (September 1980), pp. 1175–96.
12. G. E. Peterson, A. Carnevale, and U. C. Paek, "Comparison of Vector and Scalar Modes in a Lightguide with a Hyperbolic Secant Index Distribution," B.S.T.J., *59*, No. 9 (November 1980), pp. 1681–91.
13. G. E. Peterson, A. Carnevale, U. C. Paek, and J. W. Fleming, "Numerical Calculation of Optimum α for a Germania-Doped Silica Lightguide," B.S.T.J., *60*, No. 4 (April 1981), pp. 455–70.
14. U. C. Paek, G. E. Peterson, and A. Carnevale, "Dispersionless Single-Mode Lightguides with α Index Profiles," B.S.T.J., *60*, No. 5 (June 1981), pp. 583–98.
15. U. C. Paek, G. E. Peterson, and A. Carnevale, "Electromagnetic Fields, Field Confinement, and Energy Flow in Dispersionless Single-Mode Lightguides with Graded-Index Profiles," B.S.T.J., *60*, No. 8 (October 1981), pp. 1727–43.
16. Y. Kokubun and K. Iga, "Mode Analysis of Graded-Index Optical Fibers Using a Scalar Wave Equation Including Gradient-Index Terms and a Direct Numerical Integration," J. Opt. Soc. Am., *70*, No. 4 (April 1980), pp. 388–94.
17. W. L. Mammel and L. G. Cohen, "Numerical Prediction of Fiber Transmission Characteristics from Arbitrary Refractive-Index Profiles," Appl. Opt., *21*, No. 4 (February 1982), pp. 699–703.
18. S. J. Jang, L. G. Cohen, W. L. Mammel, and M. A. Saifi, "Experimental Verification of Ultra-Wide Bandwidth Spectra in Doubly-Clad Single-Mode Fiber," B.S.T.J., *61*, No. 3 (March 1982), pp. 385–90.
19. L. G. Cohen, W. L. Mammel, and S. Lumish, "Tailoring the Shapes of Dispersion Spectra to Control Bandwidths in Single-Mode Fibers," Optics Letters, *7*, No. 4 (April 1982), pp. 183–5.
20. K. Ikamoto and T. Okoshi, "Vectorial Wave Analysis of Inhomogeneous Optical Fibers Using Finite Element Method," IEEE Trans., *MTT-26* (February 1978), pp. 109–14.
21. C. Yeh, K. Ha, S. B. Dong, and W. P. Brown, "Single-Mode Optical Waveguides," Appl. Opt., *18*, No. 10 (May 1979), pp. 1490–504.
22. D. S. Burnett, *Finite Element Analysis, From Concept to Applications*, New York: Addison-Wesley, to be published.
23. M. Reed and B. Simon, *Methods of Modern Mathematical Physics IV: Analysis of Operators*, New York: Academic Press, 1978.

24. M. Abramowitz and I. A. Stegun, *Handbook of Mathematical Functions*, Washington, D. C.: National Bureau of Standards, 1970, Chapter 9.
25. O. C. Zienkiewiez, *The Finite Element Method, 3rd Edition*, England: McGraw-Hill, 1977, p. 537.
26. T. Kato, *Perturbation Theory for Linear Operators*, New York: Springer-Verlag, 1966, p. 125 and p. 391.
27. J. W. Fleming, "Material Dispersion in Lightguide Glasses," Elect. Lett., *14*, No. 11 (May 1978), pp. 326–8.
28. S. E. Miller and A. G. Chynoweth, ed., *Optical Fiber Telecommunications*, New York: Academic Press, 1979, Chapter 7, p. 188.
29. W. T. Anderson, private communication.
30. P. L. Chu and T. Whitbread, "Measurement of Stresses in Optical Fiber and Preform," Appl. Opt., *21*, No. 23 (December 1, 1982), pp. 4241–5.
31. M. J. Saunders, "A Comparison of Single-Mode Refractive Index Profiles in Preforms and Fibers," 8th ECOC, paper C-17 (September 1982).
32. K. I. White, "Design Parameters for Dispersion-Shifted Triangular-Profile Single-Mode Fibers," Elect. Lett., *18*, No. 17 (August 19, 1982), pp. 725–7.

APPENDIX

Gradient Index Terms

Gradient index terms, involving the quantity $q_r = d/dr \ln k^2$, occur in eqs. (10) and (21). Although the index or its derivative may be discontinuous, they can be approximated by smooth functions, so k^2 and g_r can be taken as well defined, continuous functions of r. This appendix concerns the changes needed in the T matrix to accommodate these terms.

Equation (10) converts to symmetric form when $h_\theta = kf$ and both sides are divided by k. The result is

$$\left(\frac{k}{r}\frac{d}{dr}\frac{r}{k^2}\frac{d}{dr}k - \frac{1}{r^2} - \frac{g_r}{r} + k^2\right)f = \beta^2 f. \tag{72}$$

Applying the Galerkin technique gives for the first term,

$$\begin{aligned} A' \sim a'_{jl} &= -\left[\frac{1}{k^2}\frac{d}{dr}(kN_l), \frac{d}{dr}(kN_j)\right]\delta^2 \\ &= \left[\left(\frac{dN_l}{dr}, \frac{dN_j}{dr}\right) + \frac{1}{4}(g_r^2 N_l, N_j)\right. \\ &\quad \left. + \frac{1}{2}\left(g_r \frac{dN_l}{dr}, N_j\right) + \frac{1}{2}\left(g_r N_l, \frac{dN_j}{dr}\right)\right]\delta^2 \end{aligned} \tag{73}$$

in place of matrix A specified in eq. (34). The first quantity is a_{jl} as before, the second adds to the C matrix of eq. (35), and the last two when evaluated by the trapezoidal rule contribute only to the first side diagonals. The term g_r/r is handled in the same way as k^2. Combining these contributions gives a new T matrix that is symmetric and tridiagonal.

Likewise, eq. (21) converts to symmetric form when $k^{1/2}f$ replaces f.

The rest proceeds in the same way to give a symmetric, tridiagonal T matrix.

Material dispersion is incorporated by expressing the index in terms of concentration functions as before. Radial derivatives needed for the gradient index terms themselves involve derivatives of the concentration function. The ω^2 derivatives of these terms, needed for the modal delays, are found by differentiating the coefficients of the concentration functions.

AUTHOR

Terrence A. Lenahan, S.B. and S.M. (Electrical Engineering) 1964, Massachusetts Institute of Technology; Ph.D. (Applied Mathematics) 1970, University of Pennsylvania; Bell Laboratories, 1970—. Mr. Lenahan has done studies of various areas of mathematical physics including electromagnetic propagation, elasticity, and fluid mechanics. He has recently been interested in the propagation of light in optical fibers. Member, American Mathematical Society, SIAM, Sigma Xi.